AIP | Journal of Applied Physics

Size dependence on the ordering process in colloidal FePt nanoparticles

J. M. Vargas, R. D. Zysler, L. M. Socolovsky, M. Knobel, and D. Zanchet

Citation: J. Appl. Phys. **101**, 023903 (2007); doi: 10.1063/1.2409620
View online: http://dx.doi.org/10.1063/1.2409620
View Table of Contents: http://jap.aip.org/resource/1/JAPIAU/v101/i2
Published by the AIP Publishing LLC.

Size dependence on the ordering process in colloidal FePt nanoparticles

J. M. Vargas and R. D. Zysler[a)]
Centro Atómico Bariloche & Instituto Balseiro, CP 8400, S. C. Bariloche, Rio Negro, Argentina

L. M. Socolovsky and M. Knobel
Instituto de Física "Gleb Wataghin," Universidade Estadual de Campinas, Campinas (SP) 13083-970, Brazil

D. Zanchet
Laboratório Nacional de Luz Síncrotron, Av. Giuseppe M. Scolfaro 10000, Campinas (SP) 13084-971, Brazil

(Received 27 July 2006; accepted 2 November 2006; published online 17 January 2007)

An alternative method to study the effects of annealing process on colloidal FePt nanoparticles (2–4 nm) has been achieved. Annealing experiments at temperatures between 773 and 1073 K under inert atmosphere flux were performed in powder samples with excess of surfactant molecules on nanoparticle surface. Transmission electron microscopy, x-ray diffraction and magnetic measurements were performed to evidence the evolution of the chemically disordered fcc to chemically ordered face-centered tetragonal phase transformation. Magnetization measurements under zero-field-cooling and field-cooling ($M_{ZFC}-M_{FC}$) conditions, and hysteresis loops are extremely sensitive to the particle size distribution and were strongly affected by the annealing treatment. © *2007 American Institute of Physics*. [DOI: 10.1063/1.2409620]

I. INTRODUCTION

The preparation of ferromagnetic nanoparticles suitable for high-density storage media represents one of the challenges in basic and applied research. The $L1_0$ FePt ordered phase has large magnetocrystalline anisotropy ($\sim 5 \times 10^7 \mathrm{erg/cm^3}$) being one of the most promising materials for ultra high magnetic recording media and related technological applications.[1–4] In the last years, great efforts have been devoted to improve the $L1_0$ ordered FePt phase in nanoparticles smaller than 10 nm.[5–8] In particular, chemical routes to synthesize the magnetic nanoparticles have generated great interest owing to the possibility to tune the particle size with rather narrow size distribution[9,10] and manipulate them afterward, forming self-assembled systems or nanostructure solids by embedding the particles in magnetic or non magnetic matrix.[11–13] However, chemical synthesis usually produces chemically disordered face-centered-cubic (fcc) structure, which can be subsequently converted to the $L1_0$ ordered FePt phase. For that, the particles are submitted to high temperatures and long annealing times, which may lead to nanoparticle aggregation and the decomposition of the organic coating.[13–17] Recently, Takahashi *et al.* found that there may be a size dependence in the ordering process of FePt nanoparticles. Where, although continuous FePt thin film was $L1_0$ perfectly ordered at 773 K, FePt nanoparticles with size smaller than 5 nm and embedded in amorphous or crystalline matrix were not ordered after annealing at 873 K for 1 h.[18,19] In FePt thin films with thicknesses between 10 and 100 nm, Shima *et al.* found that larger FePt particles are more likely to order, where a drastic change occurs in the magnetization process when their morphology change from particulate to continuous one.[20] Moreover, recent reports indicate that the initial characteristic of the nanoparticles is an important parameter and has a great influence on the final structural and magnetic properties. For example, in self-assemblies of FePt nanoparticle multlayers, Held *et al.* found a clear dependence of the structural and magnetic properties with the sample thickness.[21–23] In this article we explore the feasibility of the alternative annealing procedure that leads the desired properties, i.e. high coercive field, without external chemical or crystalline effect (induced by substrate, thicknesses or Ag doping effect). A systematic study of size, crystallinity, and magnetic properties of the produced FePt nanoparticles are presented. Our method allows one to tune the size and degree of the crystalline order with final size up to 25 nm. Potential technological consequences are significant.

II. SYNTHESIS AND ANNEALING PROCEDURE

Spherical-like nanoparticles of $Fe_{51}Pt_{49}$ (2–4 nm of diameter) were synthesized by a chemical method using inexpensive metallic precursors with good air stability and relatively low toxicity.[24] A mixture of $Pt(acac)_2$ (1.17 mmol), $FeCl_2 \cdot 4H_2O$ (1.15 mmol) and 1,2-hexadecanediol (2.36 mmol) was kept in solution with phenyl-ether (10 mL) into a reaction vessel with vigorous stirring under argon flux for 10 min and was continuously heated to 473 K. After waiting 13 min, a solution of oleic acid (10.62 mmol), oleylamine (11.21 mmol), and phenyl-ehter (10 mL) was injected and heated to 573 K for 20 min. A THF solution of superhydride (1 M, 3 mL) was slowly dropped. The system was heated under reflux at 543 K for 20 min and finally the black liquid was cooled to room temperature. After adding ethanol and centrifuging at 4000 rpm for 15 min, a black powder was obtained, which could be easily dispersed in chloroform or toluene.

a)Electronic mail: zysler@cab.cnea.gov.ar

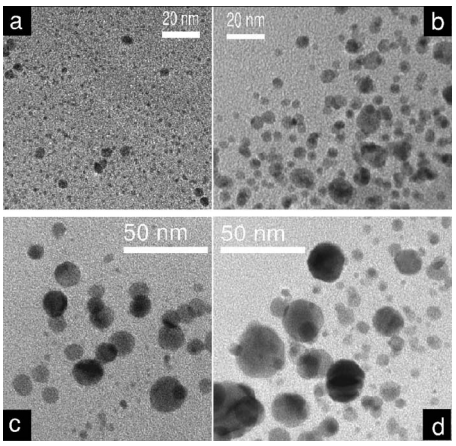

FIG. 1. TEM images of $Fe_{51}Pt_{49}$nanoparticles: (a) S-I, (b) S-II, (c) S-III, and (d) S-IV samples.

In order to study noninteracting nanoparticles, a diluted dispersion of the particles in a polymer (nonmagnetic) was made. A nominal mass dispersion close to 1% w/w was obtained when 0.004 g of precipitated nanoparticles was dispersed in 1 mL of chloroform and mixed with 0.35 g of polyethylenimine (PEY). After this, the homogeneous mixture was dried under mechanical vacuum for 1 h. An interparticle distance of $D \sim 17$ nm was estimated by using PEY ($\delta_{PEY}=1.03$ g/cm^3) and FePt ($\delta_{FePt} \sim 14.6$ g/cm^3) densities; at this mean interparticle distance the magnetic interparticle interactions are negligible. All annealing treatments were performed in an alumina crucible using the as-synthesized powder sample with an excess of surfactant molecules (metallic precursor:surfactant molar ratio close to 1:10) in a tubular furnace under continuous argon flux for 30 min at different temperatures 823, 923, and 1023 K. The annealing heating rate was fixed in 10 K/min for all treatments.

III. RESULTS AND DISCUSSION

Several transmission electron microscopy (TEM) images were taken to analyze the morphological evolution of the annealed nanoparticles from the as-synthesized samples. Figure 1 shows the morphological evolution with the annealing process. The powder sample without annealing treatment (S-I) presents a bimodal size distribution centered at 1.6 and 4.1 nm and quasispherical faceted shape [Fig. 1(a)]. Annealing the particles at 823 K for 30 min (S-II) produces the stabilization of the 4.1 nm nanoparticles with a lognormal distribution and $\sigma=0.25$ [Fig. 1(b)]. When the annealing temperature was kept at 923 K for 30 min (S-III), the size of the particles grows up to 7.0 nm with $\sigma=0.55$ [Fig. 1(c)]. At 1023 K and 30 min (S-IV) the mean size does not change significantly compared to the S-III sample 7.1 nm and there is just a small increment in the dispersion, $\sigma=0.65$ [Fig. 1(d)]. In Fig. 2 the size distribution for all samples is plotted.

The crystalline transformation from the chemical disordered fcc phase to the chemically ordered face-centered tetragonal (fct) phase was studied by x-ray diffraction (XRD). The XRD experiments were performed at the Laboratorio Nacional de Luz Sincrotron, Campinas, Brazil, in the D12A-XRD1 beamline. The x-ray wavelength was fixed in λ

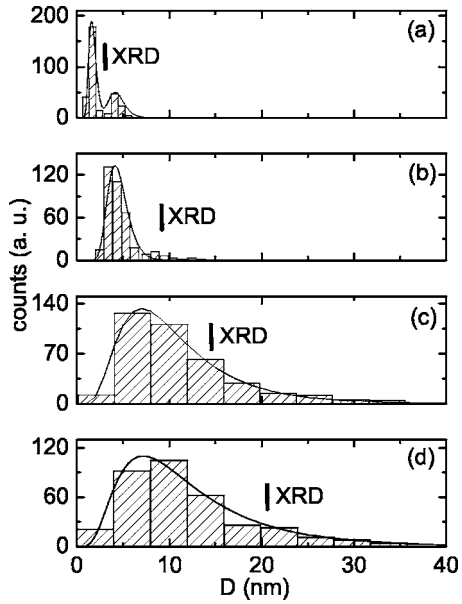

FIG. 2. Size distribution of the $Fe_{51}Pt_{49}$ nanoparticles derived from the TEM images: (a) S-I, (b) S-II, (c) S-III, and (d) S-IV samples. The continuous lines correspond to a lognormal function fitting. The volume average crystalline sizes obtained by using the Scherrer formula from the XRD experiments is also indicated.

$=0.17549$ nm ($E=7065\pm4.4$ eV) with the scattering vector $q=(4\pi/\lambda)\sin(\theta)$ in the range of $15-60$ nm^{-1}. As can be seen in Fig. 3, clear trends are evident. The XRD pattern of the sample S-I corresponds to the chemical disordered fcc phase where the characteristic superstructure peaks (001) and (110) are absent [Fig. 3(a)]. Chemical order is achieved by the annealing treatment and it improves with increased annealing temperature. In addition, from S-I to S-IV, the diffraction peaks become sharper and the $L1_0(220)/(202)$ peak splitting increases. The evolution of the mean crystalline domain size could be followed and the volume average crystalline domain size (D_X) was calculated by the Scherrer formula[25] applied to the principal peak (111). In Fig. 2 these values are signed. Table I summarizes the crystalline domain size achieve after each annealing treatments and their comparison with the TEM particle size (D_T) characterization. Since the diffraction analysis gives a volume average value for the mean crystalline domain size, we estimated a volume average particle size (D_{TW}) from the TEM histograms. It can be

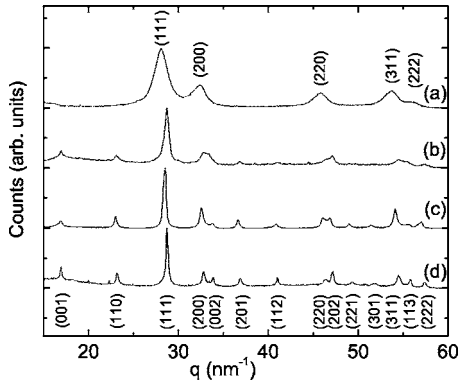

FIG. 3. XRD scans of $Fe_{51}Pt_{49}$ nanoparticles for the (a) S-I, (b) S-II, (c) S-III and (d) S-IV samples.

TABLE I. Morphological, structural and magnetic parameters obtained for the as prepared and annealed samples of $Fe_{51}Pt_{49}$ nanoparticles.

	TEM results		XRD results			Magnetization results		
Sample	D_T (nm)	D_{TW} (nm)	D_X (nm)	c/a	S	T_{max} (K)	x_{L1}	K (erg cm)$^{-3}$
S-I	1.6–4.1 ($\sigma<0.20$)	4.1	3.0	0.995	0	14.5	0	2×10^6
S-II	4.1 ($\sigma=0.25$)	13.6	9.4	0.976	0.16	120	0.17	1.4×10^7
S-III	7.0 ($\sigma=0.55$)	21.1	14.5	0.968	0.59	239	0.44	—
S-IV	7.1 ($\sigma=0.65$)	23.9	20.3	0.973	0.83	$\gg$320	0.75	—

seen that the crystalline domains are smaller than the average particle sizes for samples S-I, S-II, and S-III, which indicates the presence of defects of multiple-domain particles. Interesting, for sample S-IV, both values are similar, pointing out that at 1023 K, the particle size does not increase significantly, but the crystalline order does. This will strongly affect the magnetic property, as described bellow. From the respective diffraction pattern for sample S-I to S-IV and considering the peak reflection (111) and (200), the variation of the lattice parameters a and c were followed. The variation of both parameters, decrease continuously from 0.388 nm (S-I) to 0.382 nm (S-IV) and 0.386 nm (S-I) to 0.372 nm (S-IV), respectively. The c/a ratio was calculated and showed in Table I. The generalize Bragg and Williams long-range order parameter S which describes the ratio of the $L1_0$ phase ($S=0$ for completely random arrangement and $S=1$ for complete chemical order) was obtained by comparing the integrated intensity of the superstructure reflection (110) with that of a fundamental reflection (200).[26,27] The value of S increase continuously as the annealing temperature increase, reached 83% for the ordered $L1_0$ phase in the S-IV sample (see Table I).

Figure 4 shows the magnetization curves as a function of temperature measured under zero field cooling (ZFC) and field cooling (FC) conditions, applying a magnetic field of $H=20$ Oe, for the as-prepared sample dispersed in PEY (DS) (a) and powder sample S-I (b), S-II (c), S-III (d), S-IV (e). DS and S-I samples present similar curves, typical for single domains of noninteracting systems where the ZFC and FC magnetization curves superimpose at high temperatures and, below the irreversibility temperature, the ZFC magnetization presents a maximum whereas the FC magnetization curve increases monotonically with decreasing temperature [Figs. 4(a) and 4(b)].[28] The irreversibility temperature and the maximum of the ZFC magnetization are similar for both samples. This would be explained by the existence of a large amount of surfactant molecules in the S-I sample, that also keeps the particles far apart and hinders the interparticle magnetic interactions. In both DS and S-I magnetization curves, we observe only the blocking of the 4 nm particles because the smaller ones (2 nm) have the blocking temperature below $T=2$ K. Samples annealed at different temperatures show a systematic variation of the magnetic properties with the treatment. The samples S-II and S-III present an anomalous variation in the ZFC-FC magnetization curves, close to 126 and 249 K, respectively, possibly owing to the difference between both crystalline and morphological dynamical evolution [Figs. 4(c) and 4(d)]. For the sample S-IV, a continuous variation of the ZFC-FC magnetization curves is observed, suggesting a better crystalline and morphological homogeneity [Fig. 4(e)]. Furthermore, all annealed samples are blocked at room temperature since their size distribution enlarge.

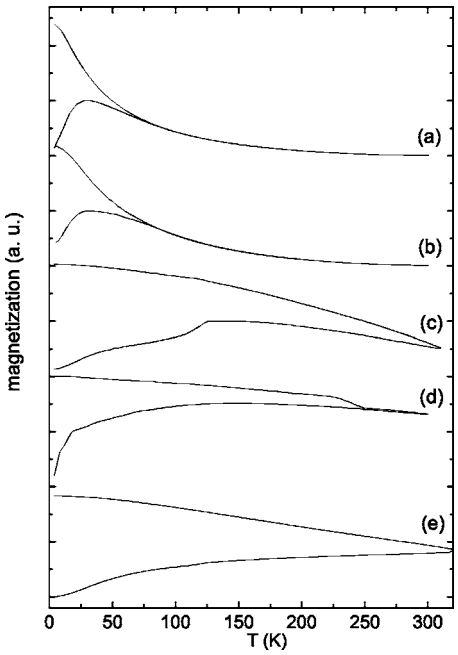

FIG. 4. $M(T)$ curves measured under ZFC-FC conditions applying a field $H=20$ Oe for the $Fe_{51}Pt_{49}$ nanoparticles: (a) dispersed S-I, (b) powder S-I, (c) S-II, (d) S-III, and (e) S-IV samples.

For weakly interacting nanoparticles the energy barrier distribution $f(T)$ can be calculated from the $M_{ZFC}(T)$ and $M_{FC}(T)$ curves:

$$Tf(T) = \frac{d(M_{ZFC} - M_{FC})}{dT}. \quad (1)$$

This $f(T)$ function presents a maximum at certain temperature that corresponds to the blocking temperature of the particles with the mean size. Table I summarizes the values of T_{max} for all samples. In the annealed samples, because of the existence of nonzero coercive field up to room temperature and the possible presence of the interparticle interactions, the obtained $f(T)$ curve is only an approximation to the size distribution function. If the mean magnetic volume per nanoparticle (V_m) is known, by the temperature associated to the maximum value of the $Tf(T)$, T_{max}, it is possible to estimate the value of the effective anisotropy constant (K) according to the Neél-Brown formula:[29]

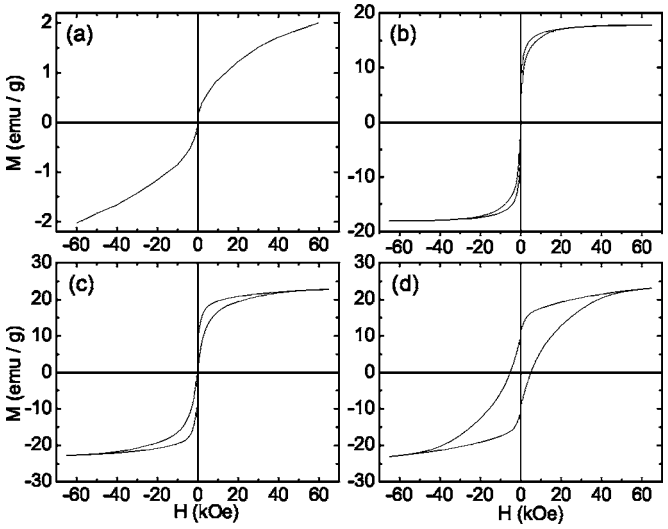

FIG. 5. Hysteresis loops measured at $T=320$ K: S-I (a), S-II (b), S-III (c), and S-IV (d). The magnetization unit is emu per total sample mass (NPs +surfactants).

$$28k_BT_{\max} = KV_m, \tag{2}$$

where the factor 28 correspond to the logarithmic fraction between the measuring time ($\sim$100 s for dc magnetization measurements) and the characteristic relaxation time ($\sim 10^{-10}$ s), and k_B is the Boltzmann constant. Using a mean diameter of 4.1 nm for the S-I and S-II samples we have obtained the values of $K_I = 2\times 10\ \mathrm{erg/cm^3}$ and $K_{II} = 1.4\times 10^7\ \mathrm{erg/cm^3}$, respectively. The 2 nm particles in the as-prepared sample have not been considered because there are in superparamagnetic regime up to $T=4$ K.

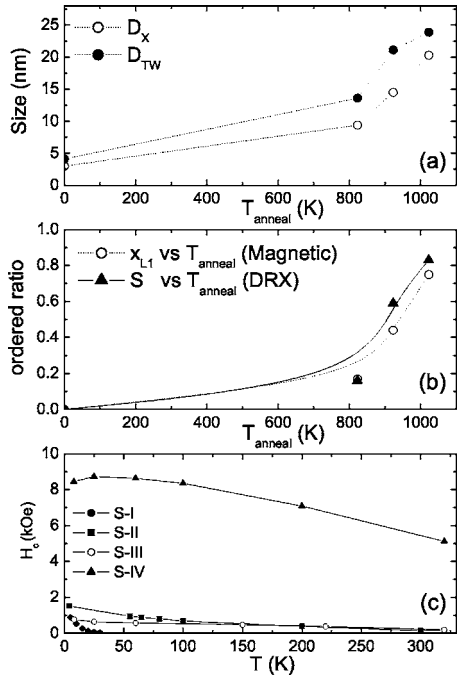

FIG. 6. (a) Development of the morphological and crystalline size where the bar in the solid symbols correspond to the lower and bigger TEM sizes, (b) The fraction of the $L1_0$ phase (S and x_{L1}), and (c) variation of the coercive field for each annealed sample as a function of the annealing temperature (T_{anneal}).

Figure 5 shows the hysteresis loops measured at 320 K for all samples (Fig. 5). It is clear from Fig. 5(a) that the S-I sample contains nanoparticles in superparamagnetic regime at room temperature as well as a significant amount of material which does not reach the saturation even at the applied field $H=60$ kOe. This nonsaturation could be associated to the existence of small nanoparticles ($\sim$2 nm). All annealed samples have magnetization curves that saturate at 60 kOe. This fact suggests that most of the smaller nanoparticles disappear constituting bigger particles, in agreement with TEM and XRD measurement. Interesting, the magnetization of the annealed samples presents both superparamagnetic and blocked (irreversible) contributions. This phenomenon suggests that the crystalline transformation to the ordered $L1_0$ phase is only partial, i.e., the high anisotropy $L1_0$ phase is blocked at room temperature and the nontransformed soft fcc phase remains in a superparamagnetic regime. The superposition of both trends explains the anomalous loops shape observed with a narrowing at low magnetic fields. From the respective loops measured at 4 and 320 K it is possible to estimate the fraction of the hard magnetic material present in the particles x_{L1}:[30]

$$x_{L1} = \frac{\oint_{320\ \mathrm{K}} MdH}{\oint_{4\ \mathrm{K}} MdH}, \tag{3}$$

where each integral corresponds to the subtended area in the loops measured at 320 and 4 K, respectively. Table I summarizes the evolution of x_{L1} with the annealing temperature. Indeed, the annealing treatment produces the crystalline phase transformation. Then, the nature of the magnetocrystalline anisotropy would be gradually modified to expected values from chemically disordered fcc to chemically ordered fct. Compared to the S fraction obtained by XRD, the agreement was excellent. In Fig. 6 we have summarized the morphological, crystalline, and magnetic behavior after thermal treatments. As the annealing temperature increases, the morphological and crystalline domain sizes of nanoparticles show a continuous increment [Fig. 6(a)]. Also the fraction of the $L1_0$ phase become predominant as the annealing temperature increases [Fig. 6(b)]. Figure 6(c) shows the temperature dependence of the coercive field (H_C) for the S-I and annealing samples, where an abrupt increment of H_C is observed for the annealing sample at 1023 K evidencing the stabilization of the ordered fct crystalline phase.

IV. CONCLUSION

In the present work we developed an alternative method to obtain FePt nanoparticles with desired properties and we investigated the morphological, crystalline structure, and magnetic properties of as-prepared sample (4 nm $Fe_{51}Pt_{49}$ nanoparticles) and thermally treated samples. This methodology is an insightful way to study the correlation between morphological, crystalline, and magnetic properties without any substrate or self-assembled induced effect. Although self-organized nanoparticles in multilayers are the desirable

condition for studying the magnetism evolution, the substrate may have strong effect in the final crystalline and magnetic properties.

TEM measurements showed a continuous increment of size with the annealing temperature reaching up to 25 nm. As the annealing temperature increases, the superlattice diffraction peaks appear and grow, and some of the fundamental peaks split. The peak splitting was associated to the increment of the crystalline order and the peak sharpening due to nanoparticle growing. A strong correlation between morphological and crystalline size was observed, i.e., as the size of nanoparticles increases by the annealing, the chemical order fct phase was progressively achieved. Magnetic loops and ZFC-FC magnetization curves show that annealing samples are blocked at room temperature due to the particle size growing and the enlargement of the anisotropy energy by the $L1_0$ phase presence. From the magnetization loops measured at $T=4$ K and $T=320$ K we have extracted the evolution of the chemically disordered fcc to chemically ordered fct phase transformation with annealing treatments, in excellent agreement with the x-ray diffraction data. Afterward each annealing process, both size grow and crystalline transformation were clearly observed from the magnetic characterization pointing out that, annealing the sample at 1023 K, the particle size does not increase significantly, but the crystalline order does. This stabilization effect and the crystalline and morphological homogeneity enhancement could be explained by the total degradation of the surfactant molecules, avoiding the coalescence between particles. Therefore, as a possible mechanism for achieve the total $L1_0$ crystalline phase, avoiding enlargement of the size distribution, higher annealing temperatures in short annealing times may be perform.

ACKNOWLEDGMENTS

The authors would like to acknowledge the support of ANPCyT-Argentina (PICT 03–13297), Conicet-Argentina (PIP5250), Brazil-Argentina cooperation project BR/PA03-EIII/004, and LNLS D10A-XRD2 No. 4053/05 and D11A-SAXS No. 4050/05 projects.

[1] A. Moser, K. Takano, D. T. Margulies, M. Albrecht, Y. Sonobe, Y. Ikeda, S. Sun, and E. E. Fullerton, J. Phys. D **35**, R157 (2002).
[2] S. B. Darling and S. D. Bader, J. Mater. Chem. **15**, 4189 (2005).
[3] Y. Jun, Y. Huh, J. Choi, J. Lee, H. Song, S. Kim, S. Yoon, K. Kim, J. Shin, J. Suh, and J. Cheon, J. Am. Chem. Soc. **127**, 5732 (2005).
[4] J. C. Bertolini and J. Massardier, Catal. Lett. **9**, 183 (1991).
[5] S. Sun, C. B. Murray, D. Weller, L. Folks, and A. Moser, Science **287**, 1989 (2000).
[6] I. Zafiropoulou, V. Tzitzios, D. Petridis, E. Devlin, J. Fidler, S. Hoefinger, and D. Niarchos, Nanotechnology **16**, 1603 (2005).
[7] S. Kang, J. W. Harrell, and D. E. Nikles, Nano Lett. **2**, 1033 (2002).
[8] T. S. Vedantam, J. P. Liu, H. Zeng, and S. Sun, J. Appl. Phys. **93**, 7184 (2003).
[9] M. Chen, J. P. Liu, and S. Sun, J. Am. Chem. Soc. **126**, 8394 (2004).
[10] J. M. Vargas and R. D. Zysler, Nanotechnology **16**, 1474 (2005).
[11] H. Zeng, S. Sun, R. L. Sandstrom, and C. B. Murray, J. Magn. Magn. Mater. **266**, 227 (2003).
[12] F. Iskandar, T. Iwaki, T. Toda, and K. Okuyama, Nano Lett. **5**, 1525 (2005).
[13] A. C. C. Yu, M. Mizuno, Y. Sasaki, M. Inoue, H. Kondo, I. Ohta, D. Djayaprawira, and M. Takahashi, Appl. Phys. Lett. **82**, 4352 (2003).
[14] S. Yamamoto, Y. Morimoto, T. Ono, and M. Takano, Appl. Phys. Lett. **87**, 032503 (2005).
[15] M. Mizuno, Y. Sasaki, A. C. C. Yu, and M. Inoue, Langmuir **20**, 11305 (2004).
[16] V. Tzitzios, D. Niarchos, G. Hadjipanayis, E. Devlin, and D. Petridis, Adv. Mater. (Weinheim, Ger.) **17**, 2188 (2005).
[17] H. Zeng, J. Li, Z. L. Wang, J. P. Liu, and S. Sun, IEEE Trans. Magn. **38**, 2598 (2002).
[18] Y. K. Takahashi, T. Ohkubo, M. Ohnuma, and K. Hono, J. Appl. Phys. **93**, 7166 (2003).
[19] R. V. Chepulskii and W. H. Butler, Phys. Rev. B **72**, 134205 (2005).
[20] T. Shima, K. Takanashi, Y. K. Takahashi, and K. Hono, Appl. Phys. Lett. **81**, 1050 (2002).
[21] G. A. Held, H. Zeng, and S. Sun, J. Appl. Phys. **95**, 1481 (2004).
[22] T. Thomson, B. D. Terris, M. F. Toney, S. Raoux, J. E. E. Baglin, S. L. Lee, and S. Sun, J. Appl. Phys. **95**, 6738 (2004).
[23] M. Müller and K. Albe, Phys. Rev. B **72**, 094203 (2005).
[24] S. Sun, S. Anders, T. Thomson, J. E. E. Baglin, M. F. Tuney, H. F. Hamnann, C. B. Murray, and B. D. Terris, J. Phys. Chem. B **107**, 5419 (2003).
[25] R. M. Cornell and U. Schwermann, *The Iron Oxides: Structure, Properties, Reactions, Occurrence and Uses* (VCH, New York, 1996), p. 57.
[26] B. E. Warren, *X-Ray Diffraction* (Dover, New York, 1969).
[27] S. Anders, M. F. Toney, T. Thomson, R. F. C. Farrow, J.-U. Thielve, B. D. Terris, S. Sun, and B. Murray, J. Appl. Phys. **93**, 6299 (2003).
[28] J. M. Vargas, W. C. Nunes, L. M. Socolovsky, M. Knobel, and D. Zanchet, Phys. Rev. B **72**, 184428 (2005).
[29] A. J. L. Dormann, L. Bessais, and D. Fiorani, J. Phys. C **21**, 2015 (1988).
[30] L. Tauxe, T. A. T. Mullender, and T. Pick, J. Geophys. Res. **101**, 571 (1996).